The American Journal of Pathology

Cecal tumorigenesis in AhR-deficient mice depends on cecum-specific MAPK pathway activation and inflammation.

Hisanori Matoba[1,6], Masaya Takamoto[2*], Chifumi Fujii[1,3**], Masatomo Kawakubo[1], Eriko Kasuga[4], Tomio Matsumura[5], Tatsuya Natori[4], Ken Misawa[6], Shun'ichiro Taniguchi[7], and Jun Nakayama[1]

1. Department of Molecular Pathology, Shinshu University School of Medicine, Asahi 3-1-1, Matsumoto 390-8621, Japan
2. Department of Infection and Host Defense and Pathobiology, Shinshu University School of Medicine, Asahi 3-1-1, Matsumoto 390-8621, Japan
3. Department of Advanced Medicine for Health Promotion, Institute for Biomedical Sciences, Interdisciplinary Cluster for Cutting Edge Research, Shinshu University, Asahi 3-1-1, Matsumoto 390-8621, Japan
4. Department of Laboratory Medicine, Shinshu University Hospital, Asahi 3-1-1, Matsumoto 390-8621, Japan
5. Anaeropharma Science Incorporated, Asahi 3-1-1, Matsumoto 390-8621, Japan
6. Department of Pathology, Ina Central Hospital, Koshiroukubo 1313-1, Ina 396-8555, Japan
7. Department of Comprehensive Cancer Therapy, Shinshu University School of Medicine, Asahi 3-1-1, Matsumoto 390-8621, Japan

Number of text pages: 48 pages.
Number of tables/figures: 4 tables and 8 figures.

A short running head: MAPK activation in *Ahr*-/- cecal tumors.

Grant numbers and source of support: This study was partly funded by the grant from Shinshu Public Utility Foundation for Promotion of Medical Sciences (to HM), and also partly funded by Grants-in-Aids for Scientific Research (C) JP18K08613 (to CF), (B) JP15H04712 and 19H03441 (to JN) from the Japan Society for the Promotion of Science.

Disclosures: None declared.

*Correspondence to Masaya Takamoto

Address: Department of Infection and Host Defense and Pathobiology, Shinshu University School of Medicine, Asahi 3-1-1, Matsumoto 390-8621, Japan.
Email: masaya@shinshu-u.ac.jp
Tel: +81-263-37-2625
Fax: +81-263-37-3092

**Correspondence to Chifumi Fujii
Address: Department of Molecular Pathology, Shinshu University School of Medicine, Asahi 3-1-1, Matsumoto 390-8621, Japan.
Email: chifumif@shinshu-u.ac.jp
Tel: +81-263-37-3395
Fax: +81-263-37-2581

Abstract

The aryl hydrocarbon receptor (AhR) is a transcription factor known as a dioxin receptor. Recently, *Ahr*-/- mice were revealed to develop cecal tumors with inflammation and Wnt/β-catenin pathway activation. However, some groups reported discrepant results regarding whether β-catenin degradation is AhR-dependent. To determine whether other signaling pathways function in *Ahr*-/- cecal tumorigenesis, we investigated histological characteristics of the tumors, cytokine/chemokine production in tumors and *Ahr*-/- peritoneal macrophages. We also assessed AhR expression in human colorectal carcinomas. Ten of 28 *Ahr*-/- mice developed cecal lesions by 50 weeks of age, an incidence significantly lower than previously reported. Cecal lesions of *Ahr*-/- mice developed from serrated hyperplasia to adenoma/dysplasia-like neoplasia with enhanced proliferation. We also observed macrophage and neutrophil infiltration into the lesions early in serrated hyperplasia, although adjacent mucosa was devoid of inflammation. *Il-1b, Il-6, Ccl2*, and *Cxcl5* were upregulated at lesion sites, while only IL-6 production increased in *Ahr*-/- peritoneal macrophages following LPS+ATP stimulation. Neither *c-Myc* upregulation nor β-catenin nuclear translocation was observed unlike previously reported. Interestingly, we detected enhanced phosphorylation of Erk, Src, and EGFR and *Amphiregulin* upregulation at *Ahr-/-* lesion sites. In human serrated lesions, however, AhR expression in epithelial cells was upregulated despite morphological similarity to *Ahr*-/- cecal lesions. Our results suggest novel mechanisms underlying *Ahr*-/- cecal tumorigenesis,

depending primarily on cecum-specific MAPK pathway activation and inflammation.

Introduction

The aryl hydrocarbon receptor (AhR) is a ligand-activated transcription factor known as a dioxin receptor and is a member of the basic helix-loop-helix/Per-AhR nuclear translocator-Sim homology superfamily. On ligand binding, AhR translocates to the nucleus and induces transcription of target genes like *CYP1A1* in order to detoxify low molecular organic compounds[1]. However, AhR cannot detoxify dioxins such as 2,3,7,8-tetrachlorobenzo-p-dioxin (TCDD) and mediate their harmful effects oppositely through downstream targets[2–4].

AhR reportedly suppresses the immune response in the context of innate and adaptive immunity[5]. In particular, AhR suppresses caspase-1 activation through plasminogen activator inhibitor-2 (Pai-2) and consequently antagonizes IL-1β production[6]. Moreover, AhR was recently reported to regulate intracellular β-catenin protein levels by serving as a ligand-dependent E3 ubiquitin ligase independently of APC[7,8].

Previous reports showed that most AhR-deficient mice developed cecal tumors by 10 weeks of age[8,9]. Two mechanisms were suggested as underlying tumorigenesis in these mice: Wnt/β-catenin pathway activation and severe inflammation accompanied by IL-1β and IL-6 upregulation and subsequent Stat3 phosphorylation. Mice deficient in both AhR and apoptosis-associated speck-like protein containing a caspase recruitment domain (ASC) showed considerably reduced tumor incidence relative to *AhR* single knockouts due to suppressed inflammasome activation[9]. Also, germ-free AhR-deficient mice do not show tumor

development, suggesting that inflammation caused by gut microbiota is important for tumorigenesis[9].

Initially AhR activity was reported to promote β-catenin degradation[7,8], but later studies reported discrepant results[10–12]. For example, Jin et al. reported that TCDD and tryptophan metabolites did not alter β-catenin levels in CaCo-2 cells through AhR[11], suggesting that other signaling pathways underlie cecal tumorigenesis in *Ahr*-/- mice.

To investigate these discrepancies, we undertook detailed analysis of tumorigenesis in AhR-deficient mice. We revealed that MAPK signaling was activated primarily at lesion sites of *AhR*-/- mice based on the morphological similarity between *AhR*-/- cecal lesions and human colorectal serrated lesions.

Materials and methods

Animal experiments

Wild-type and AhR-deficient mice[4] on a C57BL/6 background were bred and maintained under conventional conditions in the animal house of Shinshu University. AhR-deficient mice were mated with ASC-deficient mice[13] to generate *Ahr*-/- *Asc*-/- (DKO) mice. Because we maintained *Ahr*-/- mice by breeding DKO males with *Ahr*+/- *Asc*+/- females, experiments were performed using *Ahr*-/- *Asc*+/- (*Ahr*-/-), *Ahr*+/- *Asc*+/- (WT), and *Ahr*+/- *Asc*-/- (*Asc*-/-) mice. Sequences of PCR primers used for genotyping are listed in Table 1. In a time course experiment, 28 *Ahr*-

/-, 23 WT, 12 DKO, and 16 *Asc*-/- mice were sacrificed at indicated times up to 50 weeks of age. Ileocecal regions of mice were opened to confirm the presence of cecal tumors, and intestinal tissues were used for histological and quantitative RT-PCR (qRT-PCR) analysis. All animal experiments were approved by the Shinshu University Animal Care and Use Committee.

Histological analysis and immunohistochemistry (IHC)

Histological and immunohistochemical studies were performed using 3-μm thick sections from formalin-fixed, paraffin-embedded tissue blocks. Sections were stained with hematoxylin and eosin. Antibodies used for immunohistochemistry and procedures related to antibodies used in immunohistochemistry are shown in Table 2.

Tissue sections were deparaffinized and rehydrated through a series of xylene and ethanol. Endogenous peroxidase activity was blocked using 3% hydrogen peroxide (H_2O_2) in methanol for 10 minutes. Antigen retrieval was carried out by microwaving (in 10 mM Tris-HCl buffer (pH 8.0) containing 1 mM EDTA for 30 minutes) or trypsinization (digested with 0.25% trypsin 250 (Difco, Franklin Lakes, New Jersey) at 37 °C for 30 minutes) according to primary antibodies listed in Table 2. Slides were incubated with primary antibodies for 1 hour. Envision+ System (anti-rabbit) (DAKO, Santa Clara, California), Envision+ System (anti-mouse) (DAKO), or anti-rat immunoglobulin antibody conjugated with HRP (DAKO) was used as secondary antibody according to primary antibodies. Slide were incubated with secondary

antibodies for 30 minutes. For anti-Ki-67 and anti-CD3 antibodies, Histofine mouse stain kit (Nichirei Biosciences) was used for mouse-on-mouse immunostaining following manufacturer's instructions. Peroxidase activity was visualized with diaminobenzidine-H_2O_2 solution.

qRT-PCR

Total RNA was extracted from mouse intestinal tissues using an RNeasy Mini Kit (Qiagen, Hilden, Germany), and 250 ng RNA was reverse transcribed using SuperScript III (Invitrogen, Waltham, Massachusetts), random primers (Promega, Fitchburg, Wisconsin), and oligo-dT primers (Promega), following the manufacturers' instructions. qRT-PCR analysis was performed using a 7300 Real-Time PCR System (Applied Biosystems, Waltham, Massachusetts). Premixed reagents containing primers and TaqMan probes (Applied Biosystems) were used for genes listed in Table 3. SYBR Premix Ex Taq (Takara, Kusatsu, Japan) and primers were used for genes shown in Table 4. mRNA expression was normalized to that of Gapdh. ΔΔCT values and fold-expression of target genes were determined by defining mRNA expression in a WT 45-week-old female mouse as 1.0. Data are represented as means ± SD (n = 6 for *Ahr*-/- mice; n = 7 for WT mice).

PCR amplification and direct sequencing of mouse *Braf*

148 Genomic DNA was extracted from mouse intestinal tissues and tails using a High Pure PCR
149 Template Preparation Kit (Roche, Basel, Switzerland) followed by phenol chloroform
150 extraction and ethanol precipitation. Exon 18 of mouse *Braf* was amplified by PCR using the
151 primers 5'-GACAGCTTAAAAGTAGGTCGT-3' (forward) and 5'-
152 AGCCCTTCAGTGTATTTCTCG-3' (reverse). The amplification protocol was: initial
153 denaturation at 98°C for 10 seconds; 30 cycles of denaturation at 98°C for 10 seconds,
154 annealing at 55°C for 10 seconds, and extension at 72°C for 40 seconds, followed by a final
155 extension at 72°C for 4 minutes using PrimeSTAR HS DNA Polymerase (Takara). PCR
156 products were electrophoresed on 2.0% (wt/vol) agarose gels and purified using a QIAquick
157 Gel Extraction Kit (Qiagen). Subsequently, DNA sequencing reaction was performed using the
158 above forward or reverse primer with a BigDye Terminator v3.1 Cycle Sequencing Kit (Thermo
159 Fisher Scientific, Waltham, Massachusetts). Sequences were determined using a capillary
160 automatic sequencer ABI 3130XL PRISM Genetic Analyzer (Thermo Fisher Scientific).
161
162 **Macrophage preparation and stimulation**
163 *Ahr*-/- and WT peritoneal macrophages were prepared as described[14,15]. More than 90% of cells
164 obtained by this procedure were confirmed to be macrophages based on F4/80 staining.
165 Macrophages were cultivated in RPMI1640 with 10% fetal calf serum, 100 μg/mL streptomycin,
166 and 100 U/mL penicillin G with 500 ng/mL LPS (Sigma-Aldrich) for 6 h or 24 h and then

167 incubated with 2.5 mM ATP (Sigma-Aldrich) for 30 min.

168

169 **Bacterial infection**

170 *Fusobacterium nucleatum* (ATCC 25586) was cultured on Anaero Columbia Blood Agar plates
171 (BD Biosciences, Franklin Lakes, New Jersey) under anaerobic conditions, and *Escherichia*
172 *coli* (ATCC 25922) was cultured on blood agar plates (BD Biosciences). *F. nucleatum* and *E.*
173 *coli* were transferred to new plates 3 days and 1 day before infection respectively. *F. nucleatum*
174 and *E. coli* were individually suspended in physiological saline, the number of bacteria in
175 suspension was determined based on McFarland turbidity, and bacterial suspensions were
176 diluted with antibiotic-free medium to the desired multiplicity of infection (MOI). *Ahr*-/- and
177 WT peritoneal macrophages were prepared in antibiotic-free medium, and infections were
178 performed by adding diluted *F. nucleatum* or *E. coli* to macrophages for 6 h or 24 h. Ten μg/mL
179 gentamycin was added to cell cultures 1 h after infection.

180

181 **Cytokine assays**

182 Culture supernatants of peritoneal macrophages were harvested at indicated time points. IL-1β,
183 TNF, IL-6, and CCL2 concentrations were measured using a cytometric beads array flex set
184 (BD Biosciences) following the manufacturer's instructions. Data are represented as means ±
185 SD of four (LPS+ATP stimulation) and three (bacterial infection) independent experiments.

186

187 **Patients and tissue samples**

188 Specimens were obtained from 15 patients with colon tumors who underwent surgical or
189 endoscopic resection at Ina Central Hospital between 2015 and 2018. Lesions included 1 tubular
190 adenoma, 2 sessile serrated adenoma/polyps (SSA/P), 6 adenocarcinomas with adenoma
191 components, 3 adenocarcinomas with SSA/P components, and 5 adenocarcinomas without
192 adenoma or SSA/P components. In the last 5 cases without benign components, MLH1
193 immunostaining was performed to determine microsatellite instability status, and three
194 negatively-stained cases were considered to be microsatellite instability-high and to have
195 developed through the sessile serrated pathway. Use of retrospective tissue samples was
196 approved by the Ethics Committee of Ina Central Hospital, Ina, Japan.

197

198 **IHC Evaluation**

199 For IHC evaluation of mice samples, 2 high power fields (x400) (0.4mm^2) of the *Ahr*-/- lesion
200 site or the WT ileocecal region per mouse were examined for each staining except for p-Erk.
201 For Ki-67, p-Src, and p-EGFR immunostaining, positive ratios were calculated as the
202 proportion of positively stained epithelial cells relative to total number of epithelial cells. For
203 F4/80, MPO, and p-Stat3 immunostaining, we counted the total number of positively stained
204 cells per 1 mm^2. For β-catenin immunostaining, we determined the nuclear translocation ratio

as the proportion of epithelial cells showing β-catenin nuclear localization relative to total epithelial cells. For p-Erk immunostaining, h-scores of the entire *Ahr*-/- lesion site or the corresponding WT ileocecal region were assigned. To calculate the h-score, we multiplied the staining intensity in epithelial cells (none (0), weak (1), moderate (2) or strong (3)) by the percentage of positively stained cells (0 to 100%) of each intensity, resulting in a score ranging from 0 to 300. Data are represented as means ± SD.

For AhR immunostaining of human colorectal specimens, h-scores of normal colorectal mucosa, benign component (tubular adenoma, SSA/P) and the adenocarcinoma component were assigned respectively as described above. Data are represented as means ± SD.

Statistical analysis

Cumulative incidence of cecal lesions in mice was estimated by Kaplan-Meier analysis. Significance was evaluated by an unpaired 2-tailed Student's *t*-test for qRT-PCR analysis and cytokine assays. The immunohistochemical positive ratio (for Ki-67, p-Src, and p-EGFR), the number of positively stained cells per 1 mm^2 (for F4/80, MPO, and p-Stat3), the nuclear translocation ratio (for β-catenin), and the h-score (for p-Erk) of *Ahr*-/- lesion sites and WT ileocecal regions were compared using an unpaired 2-tailed Student's *t*-test. Immunohistochemical h-scores of human colorectal specimens were compared using one-way ANOVA with a Tukey-Kramer post-hoc test. All statistical data are presented as means ± SD,

and $P < 0.05$ was considered significant. All statistical analyses were performed using EZR 1.37[16] (Saitama Medical Center, Jichi Medical University, Saitama, Japan), which is a graphical user interface for R (The R Foundation for Statistical Computing, Vienna, Austria, version 3.4.1).

Results

Cecal lesions of *Ahr*-/- mice develop from serrated hyperplasia to neoplasia with macrophage and neutrophil infiltration.

We began by investigating macroscopic and microscopic cecal tumor incidence in *Ahr*-/- (*Ahr*-/- *Asc*+/-), DKO (*Ahr*-/- *Asc*-/-), WT (*Ahr*+/- *Asc*+/-), and *Asc*-/- (*Ahr*+/- *Asc*-/-) mice to compare their phenotypes with those reported previously[9]. Ten of 28 *Ahr*-/- mice developed cecal lesions by 50 weeks of age (Figure 1A). All were protuberant masses located in the cecum near the ileocecal junction (Figure 1B). None of the 12 DKO, 23 WT or 16 *Asc*-/- mice developed cecal lesions by 50 weeks of age (Figure 1A). Overall, tumor incidence of DKO mice was reduced compared with that of *Ahr*-/- mice, as previously reported[9]. Furthermore, tumor incidence of *Ahr*-/- mice was greatly reduced here relative to previous reports[8,9], even after taking heterozygosity of *Asc* allele of this experiment into consideration.

Of the 10 *Ahr*-/- mice, microscopically, cecal lesions from 9 were composed of a tumor component and a hyperplastic component (Figure 1C, E). In tumor components, glands were

243 branched and gland density was high (Figure 1G), and this component resembled human
244 colorectal high-grade adenoma/dysplasia. One of the 9 cases contained a focal adenocarcinoma
245 component invading submucosal tissue (Supplemental Figure S1A). The hyperplastic
246 component of the 9 lesions was located mainly at the periphery of the lesion site, and glands
247 exhibited serrated lumens (Figure 1E). The morphology of this component was similar to that
248 of human SSA/P, a benign precursor of the serrated pathway in colorectal tumorigenesis.
249 Therefore, we refer to this histology as ‘‘serrated hyperplasia’’. We observed severe infiltration
250 of inflammatory cells consisting mainly of macrophages and neutrophils in and under the lesion
251 site, but there was almost no inflammation apparent in the adjacent mucosa (Figure 1C, E, H).
252 Immunohistochemical analysis of lesions from *Ahr*-/- mice showed expansion of Ki-67 positive
253 cells to the full thickness of the mucosa at the tumor component, but at the hyperplastic
254 component Ki-67 positive cells had also expanded mainly on the basal side of the gland (Figure
255 1F). Ki-67 positive cells were seen only at the bottom of the crypts in colon mucosa adjacent
256 to the lesions or in normal colon mucosa of WT mice (data not shown). Based on these findings,
257 we conclude that the two components can be distinguished by the proliferative capacity. In *Ahr*-
258 /- samples, we observed neither intense nor nuclear immunostaining for β-catenin at the lesion
259 site (Figure 1D, G), even at the invasive front of the focal adenocarcinoma component
260 (Supplemental Figure S1B). Moreover, β-catenin staining were comparable in *Ahr*-/- and WT
261 mice (data not shown), unlike previously reported[8,9]. All *Ahr*-/- samples were p53-negative

(data not shown). F4/80-positive macrophages and MPO-positive neutrophils infiltrated in and under the lesion site in *Ahr*-/- samples (Figure 1H), but we observed few or no B220-positive or CD3-positive lymphocytes at this site (data not shown).

In the other one case of 10 *Ahr*-/- mice with cecal lesions, the lesion site was composed of only a hyperplastic component (Figure 2). Even so, Ki-67 positive cells had expanded mainly on the basal side of the gland (Figure 2E), and we observed cecum-specific inflammatory cell infiltration (Figure 2C, F). β-catenin nuclear translocation was not observed as well (Figure 2D).

Statistical analysis of immunostaining scores revealed that the Ki-67 positive ratio and the number of F4/80- and MPO-positive cells in a given area at an *Ahr*-/- lesion site significantly increased relative to corresponding values in the WT ileocecal region (Figure 3A-C). However, the β-catenin nuclear translocation ratio was comparable at *Ahr*-/- lesion sites and WT ileocecal regions (Figure 3D).

The distal colons of 10 *Ahr*-/- mice with cecal lesions showed various degrees of inflammation. Two of 10 cases (20%) showed severe colitis with regenerative atypia covering the distal colon (Supplemental Figure S1C). Four others (40%) showed colitis with regenerative atypia in part of distal colon (Supplemental Figure S1D). The other four cases (40%) showed only mild colitis (Supplemental Figure S1E). Interestingly, the mucosa adjacent to the lesion site was devoid of inflammation, even in cases of severe colitis. The distal colons of WT mice and *Ahr*-/- mice without cecal lesions showed almost no inflammation, except for one *Ahr*-/- mouse with severe

inflammation.

These results indicate overall that cecal lesions of *Ahr*-/- mice develop from serrated hyperplasia to neoplasia with macrophage and neutrophil infiltration.

Proinflammatory cytokines and chemokines are upregulated at lesion sites in *Ahr*-/- mice.

Based on the histological analysis, there was much evidence that cytokines and chemokines that attract inflammatory cells and increase cell proliferation were produced at lesion sites (Figure 4A). Therefore, we performed qRT-PCR analysis of transcripts encoding cytokines or chemokines and observed upregulated *Il-1b* and *Il-6* expression at lesion sites of *Ahr*-/- mice compared with the ileocecal region of WT mice (Figure 4B). *Ccl2*, *Cxcl5*, *Ccl6*, and *Ccl8* were also upregulated, consistent with macrophage and neutrophil infiltration at lesion sites. *Ifng*, *Il-12p40*, *Il-4*, and *Il-17* cytokines, which primarily regulate lymphocyte function, were not upregulated at lesion sites, consistent with the scarcity of lymphocytes (Figure 4B). Decreased expression of *Il-17* in *Ahr-/-* mice was consistent with previous reports[17,18]. We then quantified *c-Myc* mRNA expression to evaluate Wnt/β-catenin pathway activation and observed no significant differences between *Ahr*-/- and WT mice (Figure 4B). These results indicate overall that proinflammatory cytokines and chemokines are produced at lesion sites but provide no evidence of Wnt/β-catenin pathway activation.

Tissues at lesion sites of *Ahr*-/- mice exhibit enhanced Erk phosphorylation.

Given that we did not observe significant Wnt/β-catenin pathway activation in lesions from *Ahr*-/- mice, we asked what other signaling pathways might be activated in *Ahr*-/- tumorigenesis. Cecal lesions of *Ahr*-/- mice developed from serrated hyperplasia to neoplasia, and proliferating cells expanded from the bottom of crypts to full thickness in the mucosa (Figure 1, 2). We call this morphology ‘‘bottom-up morphogenesis’’, and it resembles that seen in human colorectal serrated lesions initiated by MAPK pathway activation[19]. This pattern differs from so-called “top-down morphogenesis” of human colorectal adenoma-carcinoma sequence initiated by Wnt/β-catenin pathway activation[20] (Figure 5A, B). Therefore, we evaluated MAPK pathway activation in *Ahr*-/- mice based on Erk phosphorylation. Phosphorylated Erk was strongly positive mainly in epithelial cells of most lesion sites in *Ahr*-/- mice (Figure 5C-E), and the p-Erk h-score was significantly higher at *Ahr*-/- lesions relative to WT ileocecal regions (Figure 5G). Phosphorylated Erk was weakly positive in a few epithelial cells in the terminal ileum and in colon mucosa adjacent to lesions (Figure 5F) but there was no significant difference between *Ahr*-/- and WT mice in normal intestinal mucosa (data not shown). These results suggest that MAPK pathway activation occurs primarily at lesion sites in *Ahr*-/- mice.

Tissues at *Ahr*-/- lesion sites exhibit increased phosphorylation of Src and EGFR as well as *Amphiregulin* upregulation.

Multiple studies suggest that MAPK activation at lesion sites in Ahr-/- mice depends on various pathways[21–23] (Figure 6A-B). To investigate these mechanisms more closely, we evaluated c-Src and EGFR phosphorylation at *Ahr*-/- lesion sites using immunohistochemistry and examined *Amphiregulin* expression by qRT-PCR analysis.

We observed phosphorylated Src protein in some epithelial cells at lesion sites of *Ahr*-/- mice at levels higher than that seen in adjacent mucosa (Figure 6C). Inflammatory cells present in that tissue also showed phosphorylated Src protein, although this finding could be explained by cross-reactivity of the antibody to phosphorylated Hck, Lyn, and Fyn (Figure 6C). A small number of epithelial cells in the terminal ileum and adjacent colon mucosa to lesions was also positive for phosphorylated Src (Figure 6D). The p-Src positive ratio at *Ahr*-/- lesion sites was significantly increased compared with that of WT ileocecal regions (Figure 6E), although that ratio was comparable in adjacent intestinal mucosa from both *Ahr*-/- and WT mice (data not shown). Some epithelial and inflammatory cells were positive for phosphorylated-EGFR at *Ahr*-/- lesion sites, while very few epithelial cells in the terminal ileum and adjacent colon mucosa were positive for phosphorylated-EGFR. Phosphorylated-EGFR distribution was similar to that of p-Src (Figure 6F, G), and the p-EGFR positive ratio at *Ahr*-/- lesion sites was significantly higher than that in the WT ileocecal regions (Figure 6H). *Amphiregulin* expression at *Ahr*-/- lesion sites was also upregulated relative to the WT ileocecal regions (Figure 6I).

Because *Il-6* upregulation at *Ahr*-/- lesion sites (Figure 4B) likely underlies MAPK activation,

we investigated phosphorylation of Stat3, a downstream IL-6 target that promotes cell proliferation and invasion[24,25]. In some *Ahr*-/- mice, p-Stat3 was weakly positive mainly in inflammatory cells but in a few epithelial cells at lesion sites (Figure 6J), as previously reported[9], and in some *Ahr*-/- mice there were very few or almost no p-Stat3 positive inflammatory and epithelial cells at lesion sites. The number of cells positive for phosphorylated-Stat3 at *Ahr*-/- lesion sites was somewhat higher than at WT ileocecal regions, but the difference was not statistically significant (Figure 6K).

The mouse $BRAF^{V637E}$ mutation in exon 18, which occurs at an orthologous position of the human $BRAF^{V600E}$ mutation in exon 15, reportedly induces intestinal hyperplasia and subsequent dysplasia and adenocarcinoma in mice, phenotypes that resemble the human serrated pathway[26]. To investigate whether *Braf* mutation induces MAPK activation and cecal tumorigenesis in *Ahr*-/- mice, we used direct sequencing to search for $BRAF^{V637E}$ mutations at lesion sites in four *Ahr*-/- mice but did not detect any (Supplemental Figure S2).

These results overall suggest that MAPK activation at *Ahr*-/- lesion sites is likely enhanced by synergistic EGFR phosphorylation via Src phosphorylation, *Amphiregulin* upregulation, and IL-6 production.

LPS-induced IL-6 production increases in peritoneal macrophages of *Ahr*-/- mice.

Given that adjacent mucosal tissues did not show significant Erk, Src, and EGFR

357 phosphorylation in *Ahr*-/- mice, we hypothesized that MAPK signaling seen in lesion tissues of
358 *Ahr* knockout mice might depend on inflammation at the lesion site. To investigate potential
359 functional differences between *Ahr*-/- and WT macrophages, we examined cytokine and
360 chemokine production by peritoneal macrophages after LPS+ATP stimulation. IL-6 production
361 increased in *Ahr*-/- macrophages relative to WT macrophages (Figure 7A). Although it
362 fluctuated among samples, we observed no significant difference in IL-1β production between
363 *Ahr*-/- and WT mice (Figure 7A). CCL2 production was slightly elevated in WT macrophages
364 6 h after LPS+ATP stimulation, but we observed no significant difference in TNF production
365 between *Ahr*-/- and WT mice (Figure 7A).
366 A potential explanation for our observation of decreased tumor incidence could be differences
367 in gut microbiota between different animal facilities. To investigate a potential relationship
368 between gut microbiota and intestinal inflammation, we used *Fusobacterium nucleatum*, a
369 bacteria associated with colorectal carcinogenesis[27–30], to stimulate peritoneal macrophages
370 from *Ahr*-/- and WT mice. IL-6 production increased in *Ahr*-/- macrophages by *F. nucleatum*
371 infection similarly to LPS+ATP stimulation, but changes were not statistically significant
372 possibly due to large fluctuations in values (Figure 7B). IL-1β, CCL2 and TNF production were
373 comparable in *Ahr*-/- and WT mice (Figure 7B). IL-6 production also increased in *Ahr*-/-
374 macrophages following *E. coli* infection, but the difference was not statistically significant (data
375 not shown). These results suggest that the mechanisms that promote IL-6 production in *Ahr*-/-

macrophages explain functional differences between *Ahr*-/- and WT macrophages.

AhR is upregulated in human colorectal carcinomas as lesions progress from benign precursors in both adenoma-carcinoma sequence and sessile serrated pathway.

AhR expression in epithelial cells is reportedly elevated in human colorectal carcinoma relative to normal epithelium[22]. However, given that morphology and activated signaling pathways were similar in *Ahr*-/- cecal lesions and human colorectal serrated lesions, we asked whether AhR downregulation occurred differently in tumorigenesis in the serrated pathway versus the adenoma-carcinoma sequence. To do so, we used immunohistochemstry to assess AhR expression in human colorectal carcinomas and benign precursors of both pathways. In normal colorectal mucosa, primarily interstitial cells were AhR-positive, while epithelial cells were negative (Figure 8A), as previously described[22]. In the adenoma-carcinoma sequence, AhR was weakly positive in epithelial cells of tubular adenoma and adenocarcinoma, and AhR was upregulated gradually as lesions progressed from tubular adenoma to adenocarcinoma (Figure 8B, D). In the sessile serrated pathway, AhR was weakly positive in epithelial cells of SSA/P and adenocarcinoma and upregulated gradually as lesions progressed from SSA/P to adenocarcinoma (Figure 8C, D). These findings indicate that AhR expression in epithelial cells is elevated in human colorectal carcinomas as lesions progress in both the adenoma-carcinoma sequence and the serrated pathway.

Discussion

In the present study, we revealed that cecal lesions of *Ahr*-/- mice developed from serrated hyperplasia to neoplasia with macrophage and neutrophil infiltration. The morphology of these lesions was similar to that of human colorectal serrated lesions. Tumorigenesis depended on persistent chemokine and cytokine production resulting from interactions between epithelial and inflammatory cells, activation of MAPK pathway following AhR knockout and production of cytokines such as IL-6. These results suggest novel mechanisms of *Ahr*-/- cecal tumorigenesis. By contrast, AhR expression did not decrease during tumorigenesis in both the human adenoma-carcinoma sequence and serrated pathway.

Previous reports showed that most *Ahr*-/- mice developed cecal lesions by 10 weeks of age and approximately half of DKO mice developed cecal lesions by 50 weeks of age[8,9]. Relative to that, tumor incidence of *Ahr*-/- mice in our study was significantly reduced (Figure 1A). This reduction may be due to differences in gut microbiota and resultant different susceptibility to intestinal inflammation among animal facilities. Further investigations, such as bacterial transplantation experiments, will be necessary to confirm this possibility. In addition, we did not observe Wnt/β-catenin pathway activation, which may also account for reduced tumor incidence. Several analyses report differing results regarding whether β-catenin degradation occurs through AhR[7,8,10–12], and further analysis is needed to determine under what conditions

Wnt/β-catenin pathway functions in *Ahr*-/- cecal tumorigenesis.

Cecal lesions of most *Ahr*-/- mice were composed of tumor and hyperplastic components, although one lesion was composed of the hyperplastic component only. Proliferative capacity was enhanced in the tumor component relative to the hyperplastic component (Figure 1C-H, Figure 2). These histological features indicate that serrated hyperplasia occurs initially and progresses to neoplasia by additional mutations or chromosomal aberrations. We observed macrophage and neutrophil infiltration early in serrated hyperplasia (Figure 1C-H, Figure 2), and *Il-1b*, *Il-6*, *Ccl2*, and *Cxcl5* were upregulated, consistent with persistent inflammation seen at the lesion site (Figure 4B). These results strongly suggest that progression from serrated hyperplasia to neoplasia occurs due to persistent chemokine/cytokine production brought on by interactions between epithelial and inflammatory cells (Figure 4A). The distal colons of most *Ahr*-/- mice with cecal lesions showed various degrees of inflammation (Supplemental Figure S1C-E). Therefore, ten *Ahr*-/- mice which are especially susceptible to inflammation may simultaneously develop cecal lesions and inflammation over the entire colon. However, some *Ahr*-/- mice with cecal lesions showed only mild colitis, and the mucosa adjacent to the lesion site was devoid of inflammation, even in the case with severe colitis (Figure 1C-H, Supplemental Figure S1C-E). These histological features indicate that cecal lesions of *Ahr*-/- mice develop through cecum-specific recruitment of inflammatory cells rather than from randomly generated dysplasia in the inflamed colon, and that inflammation of the distal colon

433 could be a secondary or concomitant change rather than a direct cause of cecal lesions.

434 Correspondence between genetic alterations and morphology seen in human colorectal
435 carcinoma has been reported in mouse models of colorectal cancer as well. *Apc*-mutant or
436 deficient mice, such as $Apc^{min/+}$ mice[31], develop intestinal adenomas morphologically similar to
437 so-called "top-down morphogenesis" of the human adenoma-carcinoma sequence[20,32,33] (Figure
438 5A). Enterocyte-specific knock-in of oncogenic $KRAS^{G12D}$ or $BRAF^{V637E}$ in mice leads to
439 colonic serrated lesions with "bottom-up morphogenesis" similar to human serrated
440 lesions[19,26,34] (Figure 5B). These reports show that molecular and morphological changes seen
441 in mouse colorectal tumorigenesis resemble those occurring in humans via these two pathways.
442 We found enhanced Erk phosphorylation mainly at lesion sites of *Ahr*-/- mice based on the
443 morphological similarity between *Ahr*-/- cecal lesions and human colorectal serrated lesions
444 (Figure 5, 1C-H). These results suggest that MAPK pathway activation is associated with
445 bottom-up morphology in mice colitis-associated carcinogenesis as it is in carcinogenesis of
446 $KRAS^{G12D}$ or $BRAF^{V637E}$ knock-in mouse models. Based on the morphological similarity
447 between mouse and human colorectal tumors, MAPK pathway activation may also be
448 associated with bottom-up morphology in human colitis-associated carcinogenesis as it is in
449 human serrated pathway.

450 Numerous mechanisms likely underlie MAPK pathway activation following AhR loss. A
451 cytosolic multiprotein complex including c-Src reportedly prevents AhR nuclear translocation[21].

Ligand binding to AhR triggers dissociation of a cytoplasmic multiprotein complex and subsequent release of c-Src, which moves to the membrane. Then c-Src is phosphorylated[35] presumably by the interaction with EGFR[36], and activated c-Src phosphorylate EGFR conversely[21] (Figure 6A). AhR loss seems to free c-Src and to enhance EGFR phosphorylation as is seen following AhR ligand binding (Figure 6B). Based on this notion, we found enhanced Src phosphorylation primarily at lesion sites of *Ahr*-/- mice (Figure 6C-D). Others have reported that AhR knockdown in colon cancer cells upregulates genes including amphiregulin, an EGF family member[22], and it is well known that IL-6 induces MAPK pathway activation through gp130 and SHP2[23]. Since activation of MAPK signaling, Src and EGFR phosphorylation as well as *Amphiregulin* upregulation were seen mainly at lesion sites and not to a significant extent in adjacent mucosa, and we detected no *Braf* mutations (Figure 5, 6, Supplemental Figure S2), we conclude that MAPK activation is enhanced synergistically by these mechanisms, rather than only by AhR loss in epithelial cells (Figure 6B). A similar distribution of p-EGFR- and p-Src-positive cells at *Ahr-/-* lesion sites (Figure 6C-H) supports this idea.

We also observed EGFR phosphorylation in inflammatory cells at *Ahr*-/- lesion sites, suggesting that similar mechanisms underlie EGFR phosphorylation in both epithelial and inflammatory cells. However, EGFR is reportedly phosphorylated in inflammatory cells during human gastric carcinogenesis and in mice gastric H. pylori infection model[37]. Moreover, EGFR is reportedly phosphorylated in inflammatory cells in human inflammatory bowel disease (IBD)-associated

carcinogenesis and in a mouse model of azoxymethane-dextran sodium sulfate colitis-associated carcinogenesis[38]. In these human gastrointestinal carcinogenesis and mice models, AhR does not always seem to be downregulated. Therefore, EGFR phosphorylation in inflammatory cells seems to be an important process in human and mice gastrointestinal inflammation or inflammation-associated carcinogenesis, which occur without necessarily AhR downregulation.

IL-6 production by *Ahr*-/- peritoneal macrophages increased following LPS+ATP stimulation as compared to WT macrophages, but IL-1β, CCL2, and TNF production was not (Figure 7). *Ahr* knockout reportedly enhances IL-6 and TNF production by peritoneal macrophages after LPS stimulation[39,40]. In those reports AhR-deficient mice all died within 5 weeks of age under conventional conditions, and all mice were maintained under specific pathogen-free conditions. However, in our study, *Ahr*-/- mice were maintained under conventional conditions, and only some *Ahr*-/- mice died within several weeks after birth. Therefore, difference of the environment used to house the mice and resultant macrophage differentiation between the facilities may underlie variations in TNF production. Others showed that AhR-deficient mice were hypersensitive to LPS-induced septic shock, and bone marrow-derived macrophages of AhR-deficient mice produced relatively high levels of IL-1β due to reduced Pai-2 expression[6]. Differences in IL-1β production may also be due to the environment used to house the mice. Moreover, in that report investigators stimulated macrophages with LPS only to examine IL-1β

490 production. Although monocytes (and presumably some immature macrophages) reportedly
491 produce IL-1β following LPS stimulation as they release ATP[41–43], IL-1β production via this
492 mechanism may differ somewhat from that seen in mature macrophages with ATP stimulation,
493 which activate inflammasomes overtly. Taken together, our findings suggest that IL-6
494 production is a key functional difference between *Ahr*-/- and WT macrophages, and IL-1β, TNF,
495 and CCL-2 are upregulated at lesion sites mainly by persistent inflammation itself.
496 We found that AhR is already upregulated in SSA/P, precursor lesions of human sessile serrated
497 pathway initiated by activating *BRAF* mutations (Figure 8). Previous reports showed that AhR
498 was upregulated in papillary thyroid carcinoma following establishment of activating *BRAF*
499 mutations[44,45]. However, we show that AhR is upregulated in a human adenoma-carcinoma
500 sequence in the likely absence of *BRAF* mutations (Figure 8). It is well known that activating
501 *KRAS* mutation is an essential step for progression after *APC* mutations in this pathway. In
502 addition, others reported that AhR was upregulated in tumor tissue of lung[46] and pancreatic
503 cancer[47], both of which frequently exhibit activating *EGFR* or *KRAS* mutations, and in HER2-
504 overexpressing breast cancer cells[48]. Therefore, AhR is likely upregulated downstream of
505 MAPK signaling and prevent tumorigenesis in these two pathways. In *Ahr*-/- mice, the MAPK
506 pathway is apparently activated by *AhR* knockout, whereas in the human serrated pathway and
507 the adenoma-carcinoma sequence, AhR is likely upregulated by *BRAF* or *KRAS* mutation and
508 subsequent MAPK pathway activation. However, MAPK signaling is activated initially in *Ahr*-

509 /- mice and in the human serrated pathway, while in the human adenoma-carcinoma sequence
510 MAPK pathway is activated in the middle phase of carcinogenesis by *KRAS* mutation after the
511 initial *APC* mutation[49]. The morphology of lesions in these cases are likely determined by the
512 initially activated signaling pathways respectively. Therefore, the lesions in *Ahr*-/- mice and in
513 the human serrated pathway likely show similar bottom-up serrated morphology, that is
514 somewhat different from top-down tubular morphology in the human adenoma-carcinoma
515 sequence.
516 In patients with IBD such as ulcerative colitis or Crohn's disease, colorectal carcinomas develop
517 through a dysplasia-carcinoma sequence[50], a pathway of colitis-associated carcinogenesis due
518 to chronic inflammation and resultant dysplasia formation. A classification system for subtypes
519 of dysplasia in IBD has been proposed[51], but the genetic basis of variations in dysplasia
520 morphology has not been studied in detail. AhR is reported a newly identified candidate gene
521 associated with IBD pathogenesis[52]. Therefore, further investigation is needed to determine
522 whether AhR downregulation leads to IBD-associated dysplasia or carcinoma similar to cecal
523 lesions in AhR-/- mice.
524

525 **Acknowledgement**
526 We would like to express our gratitude to Dr. Togo Ikuta for offering us AhR-deficient mice,
527 and to Dr. Elise Lamar for her critical review and editing of the manuscript.

528

529 **References**

530 1. Nguyen LP, Bradfield CA: The search for endogenous activators of the aryl
531 hydrocarbon receptor. Chem Res Toxicol 2008, 21:102–116

532 2. Nakatsuru Y, Wakabayashi K, Fujii-Kuriyama Y, Ishikawa T, Kusama K, Ide F:
533 Dibenzo[*A,L*]pyrene-induced genotoxic and carcinogenic responses are dramatically
534 suppressed in aryl hydrocarbon receptor-deficient mice. Int J Cancer 2004, 112:179–
535 183

536 3. Shimizu Y, Nakatsuru Y, Ichinose M, Takahashi Y, Kume H, Mimura J, Fujii-
537 Kuriyama Y, Ishikawa T: Benzo[a]pyrene carcinogenicity is lost in mice lacking the
538 aryl hydrocarbon receptor. Proc Natl Acad Sci U S A 2000, 97:779–782

539 4. Mimura J, Yamashita K, Nakamura K, Morita M, Takagi TN, Nakao K, Ema M,
540 Sogawa K, Yasuda M, Katsuki M, Fujii-Kuriyama Y: Loss of teratogenic response to
541 2,3,7,8-tetrachlorodibenzo-p-dioxin (TCDD) in mice lacking the Ah (dioxin) receptor.
542 Genes to Cells 1997, 2:645–654

543 5. Monteleone I, Pallone F, Monteleone G: Aryl hydrocarbon receptor and colitis. Semin
544 Immunopathol 2013, 35:671–675

545 6. Sekine H, Mimura J, Oshima M, Okawa H, Kanno J, Igarashi K, Gonzalez FJ, Ikuta T,
546 Kawajiri K, Fujii-Kuriyama Y: Hypersensitivity of aryl hydrocarbon receptor-deficient
547 mice to lipopolysaccharide-induced septic shock. Mol Cell Biol 2009, 29:6391–6400

548 7. Ohtake F, Baba A, Takada I, Okada M, Iwasaki K, Miki H, Takahashi S, Kouzmenko
549 A, Nohara K, Chiba T, Fujii-Kuriyama Y, Kato S: Dioxin receptor is a ligand-
550 dependent E3 ubiquitin ligase. Nature 2007, 446:562–566
551 8. Kawajiri K, Kobayashi Y, Ohtake F, Ikuta T, Matsushima Y, Mimura J, Pettersson S,
552 Pollenz RS, Sakaki T, Hirokawa T, Akiyama T, Kurosumi M, Poellinger L, Kato S,
553 Fujii-Kuriyama Y: Aryl hydrocarbon receptor suppresses intestinal carcinogenesis in
554 $Apc^{Min/+}$ mice with natural ligands. Proc Natl Acad Sci U S A 2009, 106:13481–13486
555 9. Ikuta T, Kobayashi Y, Kitazawa M, Shiizaki K, Itano N, Noda T, Pettersson S,
556 Poellinger L, Fujii-Kuriyama Y, Taniguchi S, Kawajiri K: ASC-associated
557 inflammation promotes cecal tumorigenesis in aryl hydrocarbon receptor-deficient
558 mice. Carcinogenesis 2013, 34:1620–1627
559 10. Braeuning A, Köhle C, Buchmann A, Schwarz M: Coordinate regulation of
560 cytochrome P450 1A1 expression in mouse liver by the aryl hydrocarbon receptor and
561 the β-catenin pathway. Toxicol Sci 2011, 122:16–25
562 11. Jin U-H, Lee S-O, Sridharan G, Lee K, Davidson LA, Jayaraman A, Chapkin RS,
563 Alaniz R, Safe S: Microbiome-Derived Tryptophan Metabolites and Their Aryl
564 Hydrocarbon Receptor-Dependent Agonist and Antagonist Activities. Mol Pharmacol
565 2014, 85:777–788
566 12. Kasai S, Ishigaki T, Takumi R, Kamimura T, Kikuchi H: β-Catenin signaling induces

CYP1A1 expression by disrupting adherens junctions in Caco-2 human colon carcinoma cells. Biochim Biophys Acta 2013, 1830:2509–2516

13. Yamamoto M, Yaginuma K, Tsutsui H, Sagara J, Guan X, Seki E, Yasuda K, Yamamoto M, Akira S, Nakanishi K, Noda T, Taniguchi S: ASC is essential for LPS-induced activation of procaspase-1 independently of TLR-associated signal adaptor molecules. Genes to Cells 2004, 9:1055–1067

14. Fujii C, Shiratsuchi A, Manaka J, Yonehara S, Nakanishi Y: Difference in the way of macrophage recognition of target cells depending on their apoptotic states. Cell Death Differ 2001, 8:1113–1122

15. Shiratsuchi A, Osada S, Kanazawa S, Nakanishi Y: Essential role of phosphatidylserine externalization in apoptosing cell phagocytosis by macrophages. Biochem Biophys Res Commun 1998, 246:549–555

16. Kanda Y: Investigation of the freely available easy-to-use software “EZR” for medical statistics. Bone Marrow Transplant 2013, 48:452–458

17. Veldhoen M, Hirota K, Westendorf AM, Buer J, Dumoutier L, Renauld JC, Stockinger B: The aryl hydrocarbon receptor links TH17-cell-mediated autoimmunity to environmental toxins. Nature 2008, 453:106–109

18. Kimura A, Naka T, Nohara K, Fujii-Kuriyama Y, Kishimoto T: Aryl hydrocarbon receptor regulates Stat1 activation and participates in the development of Th17 cells.

586 Proc Natl Acad Sci U S A 2008, 105:9721–9726

587 19. Kang M, Mitomi H, Sada M, Tokumitsu Y, Takahashi Y, Igarashi M, Katsumata T,

588 Okayasu I: Ki-67, p53, and Bcl-2 expression of serrated adenomas of the colon. Am J

589 Surg Pathol 1997, 21:417–423

590 20. Shih I-M, Wang T-L, Traverso G, Romans K, Hamilton SR, Ben-Sasson S, Kinzler

591 KW, Vogelstein B: Top-down morphogenesis of colorectal tumors. Proc Natl Acad Sci

592 U S A 2001, 98:2640–2645

593 21. Haarmann-Stemmann T, Bothe H, Abel J: Growth factors, cytokines and their

594 receptors as downstream targets of arylhydrocarbon receptor (AhR) signaling

595 pathways. Biochem Pharmacol 2009, 77:508–520

596 22. Ikuta T, Kurosumi M, Yatsuoka T, Nishimura Y: Tissue distribution of aryl

597 hydrocarbon receptor in the intestine: Implication of putative roles in tumor

598 suppression. Exp Cell Res 2016, 343:126–134

599 23. Takahashi-Tezuka M, Yoshida Y, Fukada T, Ohtani T, Yamanaka Y, Nishida K,

600 Nakajima K, Hibi M, Hirano T: Gab1 acts as an adapter molecule linking the cytokine

601 receptor gp130 to ERK mitogen-activated protein kinase. Mol Cell Biol 1998,

602 18:4109–4117

603 24. Bollrath J, Phesse TJ, von Burstin VA, Putoczki T, Bennecke M, Bateman T,

604 Nebelsiek T, Lundgren-May T, Canli Ö, Schwitalla S, Matthews V, Schmid RM,

Kirchner T, Arkan MC, Ernst M, Greten FR: gp130-Mediated Stat3 Activation in Enterocytes Regulates Cell Survival and Cell-Cycle Progression during Colitis-Associated Tumorigenesis. Cancer Cell 2009, 15:91–102

25. Grivennikov S, Karin E, Terzic J, Mucida D, Yu GY, Vallabhapurapu S, Scheller J, Rose-John S, Cheroutre H, Eckmann L, Karin M: IL-6 and Stat3 Are Required for Survival of Intestinal Epithelial Cells and Development of Colitis-Associated Cancer. Cancer Cell 2009, 15:103–113

26. Rad R, Cadiñanos J, Rad L, Varela I, Strong A, Kriegl L, Constantino-casas F, Eser S, Hieber M, Seidler B, Price S, Fraga MF, Calvanese V, Hoffman G, Ponstingl H, Schneider G, Yusa K, Grove C, Schmid RM, Wang W, Vassiliou G, Kirchner T, Mcdermott U, Liu P, Saur D, Bradley A: A genetic progression model of Braf(V600E)-induced intestinal tumorigenesis reveals targets for therapeutic intervention. Cancer Cell 2013, 24:15–29

27. Dejea CM, Wick EC, Hechenbleikner EM, White JR, Mark Welch JL, Rossetti BJ, Peterson SN, Snesrud EC, Borisy GG, Lazarev M, Stein E, Vadivelu J, Roslani AC, Malik AA, Wanyiri JW, Goh KL, Thevambiga I, Fu K, Wan F, Llosa N, Housseau F, Romans K, Wu X, McAllister FM, Wu S, Vogelstein B, Kinzler KW, Pardoll DM, Sears CL: Microbiota organization is a distinct feature of proximal colorectal cancers. Proc Natl Acad Sci U S A 2014, 111:18321–18326

624 28. Kostic AD, Gevers D, Pedamallu CS, Michaud M, Duke F, Earl AM, Ojesina AI, Jung
625 J, Bass AJ, Tabernero J, Baselga J, Liu C, Shivdasani RA, Ogino S, Birren BW,
626 Huttenhower C, Garrett WS, Meyerson M: Genomic analysis identifies association of
627 Fusobacterium with colorectal carcinoma. Genome Res 2012, 22:292–298
628 29. Castellarin M, Warren RL, Freeman JD, Dreolini L, Krzywinski M, Strauss J, Barnes
629 R, Watson P, Allen-Vercoe E, Moore RA, Holt RA: Fusobacterium nucleatum
630 infection is prevalent in human colorectal carcinoma. Genome Res 2012, 22:299–306
631 30. Yu J, Chen Y, Fu X, Zhou X, Peng Y, Shi L, Chen T, Wu Y: Invasive Fusobacterium
632 nucleatum may play a role in the carcinogenesis of proximal colon cancer through the
633 serrated neoplasia pathway. Int J Cancer 2016, 139:1318–1326
634 31. Bilger A, Shoemaker AR, Gould KA, Dove WF: Manipulation of the mouse germline
635 in the study of Min-induced neoplasia. Semin Cancer Biol 1996, 7:249–260
636 32. Oshima H, Oshima M, Kobayashi M, Tsutsumi M, Taketo MM: Morphological and
637 molecular processes of polyp formation in $Apc^{\Delta 716}$ knockout mice. Cancer Res 1997,
638 57:1644–1649
639 33. Nalbantoglu I, Blanc V, Davidson NO: Characterization of Colorectal Cancer
640 Development in $Apc^{min/+}$ Mice. Methods Mol Biol 2016, 1422:309–327
641 34. Bennecke M, Kriegl L, Bajbouj M, Retzlaff K, Robine S, Jung A, Arkan MC, Kirchner
642 T, Greten FR: Ink4a/Arf and oncogene-induced senescence prevent tumor progression

643 during alternative colorectal tumorigenesis. Cancer Cell 2010, 18:135–146

644 35. Xie G, Peng Z, Raufman J-P: Src-mediated aryl hydrocarbon and epidermal growth

645 factor receptor cross talk stimulates colon cancer cell proliferation. Am J Physiol Liver

646 Physiol 2012, 302:G1006–G1015

647 36. Belsches AP, Haskell MD, Parsons SJ: Role of c-Src tyrosine kinase in EGF-induced

648 mitogenesis. Front Biosci 1997, 2:501–518

649 37. Hardbower DM, Singh K, Asim M, Verriere TG, Olivares-Villagómez D, Barry DP,

650 Allaman MM, Washington MK, Jr. RMP, Piazuelo MB, Wilson KT: EGFR regulates

651 macrophage activation and function in bacterial infection. J Clin Invest 2016,

652 126:3296–3312

653 38. Hardbower DM, Coburn LA, Asim M, Singh K, Sierra JC, Barry DP, Gobert AP,

654 Piazuelo MB, Washington MK, Wilson KT: EGFR-mediated macrophage activation

655 promotes colitis-associated tumorigenesis. Oncogene 2017, 36:3807–3819

656 39. Kimura A, Naka T, Nakahama T, Chinen I, Masuda K, Nohara K, Fujii-Kuriyama Y,

657 Kishimoto T: Aryl hydrocarbon receptor in combination with Stat1 regulates LPS-

658 induced inflammatory responses. J Exp Med 2009, 206:2027–2035

659 40. Masuda K, Kimura A, Hanieh H, Nguyen NT, Nakahama T, Chinen I, Otoyo Y,

660 Murotani T, Yamatodani A, Kishimoto T: Aryl hydrocarbon receptor negatively

661 regulates LPS-induced IL-6 production through suppression of histamine production in

662 macrophages. Int Immunol 2011, 23:637–645

663 41. Netea MG, Nold-Petry CA, Nold MF, Joosten LAB, Opitz B, van der Meer JHM, van
664 de Veerdonk FL, Ferwerda G, Heinhuis B, Devesa I, Funk CJ, Mason RJ, Kullberg BJ,
665 Rubartelli A, van der Meer JWM, Dinarello CA: Differential requirement for the
666 activation of the inflammasome for processing and release of IL-1β in monocytes and
667 macrophages. Blood 2009, 113:2324–2335

668 42. Piccini A, Carta S, Tassi S, Lasiglie D, Fossati G, Rubartelli A: ATP is released by
669 monocytes stimulated with pathogen-sensing receptor ligands and induces IL-1β and
670 IL-18 secretion in an autocrine way. Proc Natl Acad Sci U S A 2008, 105:8067–8072

671 43. Elliott EI, Sutterwala FS: Monocytes take their own path to IL-1β. Immunity 2016,
672 44:713–715

673 44. Mian C, Ceccato F, Barollo S, Watutantrige-Fernando S, Albiger N, Regazzo D, De
674 Lazzari P, Pennelli G, Rotondi S, Nacamulli D, Pelizzo MR, Jaffrain-Rea ML,
675 Grimaldi F, Occhi G, Scaroni C: AHR over-expression in papillary thyroid carcinoma:
676 Clinical and molecular assessments in a series of Italian acromegalic patients with a
677 long-term follow-up. PLoS One 2014, 9:e101560.
678 https://doi.org/10.1371/journal.pone.0101560

679 45. Occhi G, Barollo S, Regazzo D, Bertazza L, Galuppini F, Guzzardo V, Jaffrain-Rea
680 ML, Vianello F, Ciato D, Ceccato F, Watutantrige-Fernando S, Bisognin A, Bortoluzzi

S, Pennelli G, Boscaro M, Scaroni C, Mian C: A constitutive active MAPK/ERK pathway due to $BRAF^{V600E}$ positively regulates AHR pathway in PTC. Oncotarget 2015, 6:32104–32114

46. Lin P, Chang H, Tsai W-T, Wu M-H, Liao Y-S, Chen J-T, Su J-M: Overexpression of aryl hydrocarbon receptor in human lung carcinomas. Toxicol Pathol 2003, 31:22–30

47. Koliopanos A, Kleeff J, Xiao Y, Safe S, Zimmermann A, Büchler MW, Friess H: Increased arylhydrocarbon receptor expression offers a potential therapeutic target for pancreatic cancer. Oncogene 2002, 21:6059–6070

48. Zhao S, Ohara S, Kanno Y, Midorikawa Y, Nakayama M, Makimura M, Park Y, Inouye Y: HER2 overexpression-mediated inflammatory signaling enhances mammosphere formation through up-regulation of aryl hydrocarbon receptor transcription. Cancer Lett 2013, 330:41–48

49. Morkel M, Riemer P, Bläker H, Sers C: Similar but different: Distinct roles for KRAS and BRAF oncogenes in colorectal cancer development and therapy resistance. Oncotarget 2015, 6:20785–20800

50. Warren S, Sommers SC: Pathogenesis of ulcerative colitis. Am J Pathol 1949, 25:657–679

51. Riddell RH, Goldman H, Ransohoff DF, Appelman HD, Fenoglio CM, Haggitt RC, Ahren C, Correa P, Hamilton SR, Morson BC, Sommers SC, Yardley JH: Dysplasia in

700 inflammatory bowel disease: standardized classification with provisional clinical
701 applications. Hum Pathol 1983, 14:931–968
702 52. Liu JZ, Van Sommeren S, Huang H, Ng SC, Alberts R, Takahashi A, Ripke S, Lee JC,
703 Jostins L, Shah T, Abedian S, Cheon JH, Cho J, Daryani NE, Franke L, Fuyuno Y,
704 Hart A, Juyal RC, Juyal G, Kim WH, Morris AP, Poustchi H, Newman WG, Midha V,
705 Orchard TR, Vahedi H, Sood A, Sung JY, Malekzadeh R, Westra HJ, Yamazaki K,
706 Yang SK, Consortium TIMSG, Consortium TIIG, Barrett JC, Franke A, Alizadeh BZ,
707 Parkes M, Thelma BK, Daly MJ, Kubo M, Anderson CA, Weersma RK: Association
708 analyses identify 38 susceptibility loci for inflammatory bowel disease and highlight
709 shared genetic risk across populations. Nat Genet 2015, 47:979–986
710

711 **Figure Legends**

712 **Figure 1.** Histological and immunohistochemical analysis of cecal tumorigenesis in *Ahr-/-* mice.
713 **A:** Cecal tumor incidence in *Ahr-/-* mice. **B:** Macroscopic appearance of a lesion site from *Ahr-*
714 */-* mice, which is composed of a tumor component and a hyperplastic component. (**C**-**H**)
715 Microscopic analysis of the lesion in (**B**). Panels show immunostaining for Ki-67 (**F**), F4/80
716 (**H**), MPO (**H**), and β-catenin (**D**, **G** inset). In (**C**) and (**D**), black arrowheads indicate
717 protuberant lesion site and orange arrowheads indicate adjacent mucosa. In (**E**) and (**F**) blue
718 arrowheads indicate the tumor component and yellow arrowheads indicate the hyperplastic
719 component. Scale bars, 200 μm (**C**-**D**), 100 μm (**E**-**G**), 50 μm (**H**, **G** inset).

720

721 **Figure 2.** A lesion site of *Ahr-/-* mice composed only of the hyperplastic component.
722 **A:** Macroscopic appearance of the lesion site. (**B**-**C**) Microscopic analysis of the lesion in (**A**).
723 Panels show immunostaining for β-catenin (**D**), Ki-67 (**E**), and F4/80 (**F**). Yellow arrowheads
724 indicate hyperplasia and orange arrowheads indicate adjacent mucosa in (**B**). Scale bars, 200
725 μm (**B**), 100 μm (**C**-**E**), 50 μm (**F**).

726

727 **Figure 3. Statistical analyses of β-catenin, Ki-67, F4/80, and MPO immunostaining at *Ahr-***
728 ***/-* lesion sites and WT ileocecal regions.**
729 (**A-D**) The index used to compare each antibody was calculated as described in Materials and

730 Methods. Data are represented as means ± SD. For Ki-67 immunostaining, n = 5 for *Ahr-/-* mice,
731 n = 6 for WT mice. For β-catenin, F4/80, and MPO immunostaining, n = 6 for *Ahr-/-* mice, n =
732 6 for WT mice. * $p < 0.05$, ** $p < 0.01$.

733

734 **Figure 4.** Expression of proinflammatory cytokines and chemokines at the lesion site of *Ahr-/-*
735 mice.
736 **A:** A schematic model showing development of cecal lesions in *Ahr-/-* mice. Cytokines and
737 chemokines that attract macrophages and neutrophils are continuously produced due to
738 interactions between epithelial and inflammatory cells. Proliferative activity is increased by
739 cytokines such as IL-1β and IL-6, and serrated hyperplasia progresses to adenoma and
740 adenocarcinoma. **B:** qRT-PCR analysis of indicated transcripts at the lesion site of *Ahr-/-* mice
741 and the ileocecal region of WT mice. ΔΔCT values and fold-expression of target genes were
742 determined by defining mRNA expression in a WT 45-week-old female mouse as 1.0. Data are
743 represented as means ± SD (n = 6 for *Ahr-/-* mice; n = 7 for WT mice). * $p < 0.05$, ** $p < 0.01$.

744

745 **Figure 5.** Erk phosphorylation at the lesion site of *Ahr-/-* mice.
746 (**A**-**B**) Morphogenesis of human colorectal tumors. **A:** Hematoxylin and eosin staining (left)
747 and immunostaining for Ki-67 (right) in a human tubular adenoma, representing top-down
748 morphogenesis of the adenoma-carcinoma sequence initiated by Wnt/β-catenin pathway

749 activation. **B:** Hematoxylin and eosin staining (left) and immunostaining for Ki-67 (right) in a
750 human sessile serrated adenoma/polyp, representing bottom-up morphogenesis of the human
751 serrated pathway initiated by MAPK pathway activation. **(C-F)** Immunostaining for p-Erk.
752 Purple arrowheads indicate lesion sites, and orange arrowheads indicate adjacent mucosa in (**C**)
753 and (**D**). Scale bars, 200 μm (**C**-**D**), 100 μm (**E-F**). **G:** Statistical analyses of h-score of p-Erk
754 staining between *Ahr-/-* lesion sites and WT ileocecal regions. Data are represented as means ±
755 SD (n = 5 for *Ahr-/-* mice; n = 6 for WT mice). ** $p < 0.01$.
756
757 **Figure 6.** Src phosphorylation, EGFR phosphorylation and amphiregulin expression at lesion
758 sites of *Ahr-/-* mice.
759 **A:** Schematic model showing cross-talk between AhR and EGFR signaling. A cytosolic
760 multiprotein complex including c-Src prevents AhR nuclear translocation. Ligand binding to
761 AhR leads to the dissociation of a cytosolic multiprotein complex and subsequent release of c-
762 Src, which moves to the cell membrane. Then c-Src is phosphorylated by the interaction with
763 EGFR and activated c-Src phosphorylate EGFR conversely. **B:** Schematic model showing
764 MAPK pathway activation after AhR knockdown/knockout. AhR loss frees c-Src from the
765 cytosolic multiprotein complex, allowing c-Src to move to the membrane and phosphorylate
766 EGFR, similar to AhR ligand binding shown in (A). **(C-D)** Immunostaining for p-Src. Scale
767 bars, 50 μm. **E:** Statistical analyses of p-Src positive ratio at *Ahr-/-* lesion sites and WT ileocecal

768 regions. Data are represented as means ± SD (n = 5 for *Ahr-/-* mice; n = 6 for WT mice). * $p <$
769 0.05. **(F-G)** Immunostaining for p-EGFR. Scale bars, 50 μm. **H:** Statistical analyses of p-EGFR
770 positive ratio at *Ahr-/-* lesion sites and WT ileocecal regions. Data are represented as means ±
771 SD (n = 5 for *Ahr-/-* mice; n = 6 for WT mice). ** $p < 0.01$. **I**: qRT-PCR analysis of
772 *Amphiregulin* expression at lesion sites of *Ahr-/-* mice and ileocecal regions of WT mice. ΔΔCT
773 values and fold-expression were determined by defining mRNA expression in a WT 45-week-
774 old female mice as 1.0. Data are represented as means ± SD (n = 6 for *Ahr-/-* mice; n = 7 for
775 WT mice). * $p < 0.05$. **J**: Immunostaining for p-Stat3. Scale bars, 50 μm. **K:** Statistical analyses
776 of the number of p-Stat3-positive cells at *Ahr-/-* lesion sites and WT ileocecal regions. Data are
777 represented as means ± SD (n = 6 for *Ahr-/-* mice; n = 6 for WT mice).
778
779 **Figure 7.** Cytokine and chemokine production by mouse peritoneal macrophages.
780 Production of indicated cytokines/chemokines by peritoneal macrophages of WT and *Ahr-/-*
781 mice following LPS+ATP stimulation (**A**) or *Fusobacterium nucleatum* infection (**B**). Fold
782 production is calculated by setting the mean value after 6 h of LPS stimulation at 500 ng/ml (**A**)
783 or 6 h of infection with *F. nucleatum* at a MOI = 5 (**B**) of WT mice in each experiment to 1.0.
784 Data are represented as means ± SD of quadruple (**A**) and triplicate (**B**) independent
785 experiments. * $p < 0.05$, ** $p < 0.01$, *** $p < 0.001$.
786

787 **Figure 8.** AhR immunostaining of human colorectal carcinomas and benign precursors in both
788 the adenoma-carcinoma sequence and the sessile serrated pathway.
789 (**A**-**C**) AhR immunostaining in human normal colon mucosa (**A**), the adenoma-carcinoma
790 sequence (**B**), and the sessile serrated pathway (**C**). Scale bars, 100 μm. **D:** Statistical analyses
791 of the average h-score of AhR staining between normal colon mucosa, the benign precursor
792 component, and the adenocarcinoma component in the two pathways. ** $p < 0.01$.
793

Table 1. Oligonucleotides used in genotyping

Name	Sequence
AhR-com-5s	5′-GGCGCGGGCACCATGAGCAG-3′
AhR-wt3-3as	5′-GTAGGTCAGAGCTGTCAACGAACC-3′
AhR-LacZ-3as	5′-GCGGATTGACCGTAATGGGATAGG-3′
ASC-F25SL	5′-GCCATATGTGGCCCAGTGGTAG-3′
ASC-R40	5′-TGGCTTTGGTTGGCATTGCATG-3′
ASC-LacZF1	5′-GTAGGGTTTTTCACAGACCGCT-3′

Table 2. Antibodies used in immunohistochemistry and procedures of respective antibodies

Antibodies	Clone name or Cat. No.	manufacturers	Antigen retrieval	secondary antibody	note
anti-Ki-67	B56	BD Pharmingen	microwaving	Histofine mouse stain kit	MonM
anti-β-catenin	#9562	Cell Signaling Technology	microwaving	Envision(anti-rabbit)	
anti-p53	FL-393	Santa Cruz Biotechnology Inc.	microwaving	Envision(anti-rabbit)	
anti-F4/80	CI:A3-1	Novus Biologicals	trypsinization	anti-rat immunoglobulin with HRP	
anti-MPO	ab9535	abcam	microwaving	Envision(anti-rabbit)	
anti-B220	PA3-6B2	BD Pharmingen	trypsinization	anti-rat immunoglobulin with HRP	
anti-CD3	LN10	Leica Biosystems	microwaving	Histofine mouse stain kit	MonM
anti-pErk1/2	D13.14.4E	Cell Signaling Technology	microwaving	Envision(anti-rabbit)	
anti-pSrc family	#2101	Cell Signaling Technology	microwaving	Envision(anti-rabbit)	
anti-AhR	A-3	Santa Cruz Biotechnology Inc.	microwaving	Envision(anti-mouse)	
anti-MLH1	ES05	DAKO	microwaving	Envision(anti-mouse)	
anti -pEGFR	EP774Y	Biocare Medical	microwaving	Envision(anti-rabbit)	
anti-pStat3	D3A7	Cell Signaling Technology	microwaving	Envision(anti-rabbit)	

MonM, mouse-on-mouse immunostaining

821 Table 3. Target genes and Assay IDs used in qRT-PCR analysis with premixed reagents
822 containing primers and TaqMan probes

Genes	Assay IDs
Il1b	Mm01336189_m1
Il6	Mm00446190_m1
Ccl2	Mm00441242_m1
Cxcl5	Mm00436451_g1
Ifng	Mm01168134_m1
Il10	Mm00439614_m1
Gapdh	Mm99999915_g1

831

Table 4. Target genes and sequences of the primers used in qRT-PCR analysis with SYBR Premix Ex Taq

Genes	Sense	Antisense
Ccl3	5′-CCATGACACTCTGCAACCAAG-3′	5′-AATCTTCCGGCTGTAGGAGAA-3′
Ccl4	5′-TTTCTCTTACACCTCCCGGC-3′	5′-GTCTGCCTCTTTTGGTCAGGA-3′
Ccl5	5′-GTGCTCCAATCTTGCAGTCG-3′	5′-CAGGGAAGCTATACAGGGTCAG-3′
Ccl6	5′-TTATCCTTGTGGCTGTCCTTGG-3′	5′-GGCATAAGAGAAGCAGCAGTC-3′
Ccl8	5′-CTACGCAGTGCTTCTTTGCC-3′	5′-CGTAGCTTTTCAGCACCCGA-3′
Il4	5′-TCTCGAATGTACCAGGAGCCATATC-3′	5′-AGCACCTTGGAAGCCCTACAGA-3′
Il17	5′-TCAACCGTTCCACGTCACCCT-3′	5′-AGCTTTCCCTCCGCATTGACAC-3′
Il12p40	5′-CCACTCATGGCCATGTGGG-3′	5′-GCGTGTCACAGGTGAGGTTC-3′
c-Myc	5′-GTGCTGCATGAGGAGACACC-3′	5′-GACCTCTTGGCAGGGGTTTG-3′
Gapdh	5′-GATGGGTGTGAACCACGAGA-3′	5′-GCCCTTCCACAATGCCAAAG-3′
Amphiregulin	5′-GGGGACTACGACTACTCAGAG-3′	5′-TCTTGGGCTTAATCACCTGTTC-3′

Figure 1

Matoba *et al.*

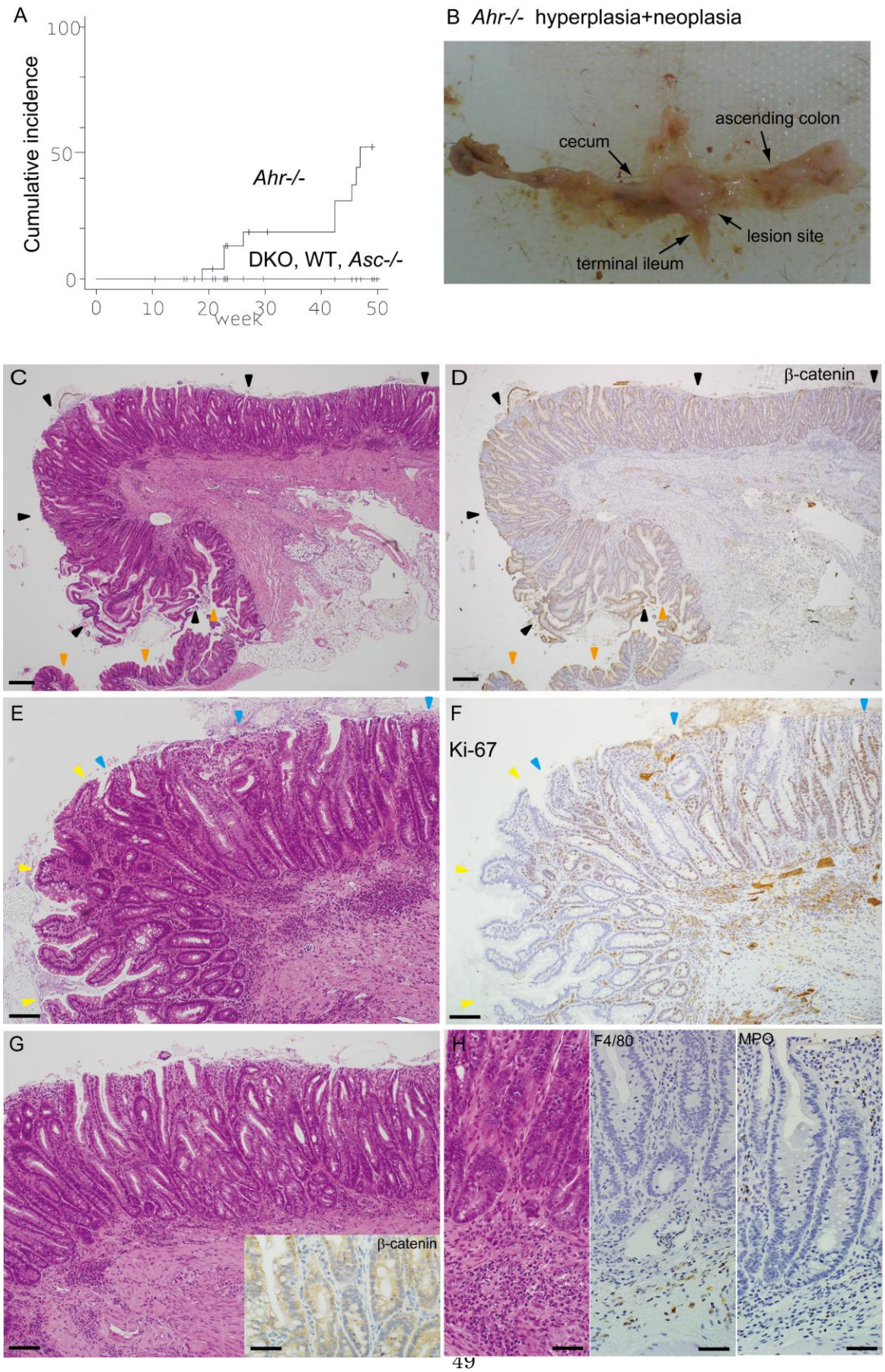

Figure 2

Matoba *et al.*

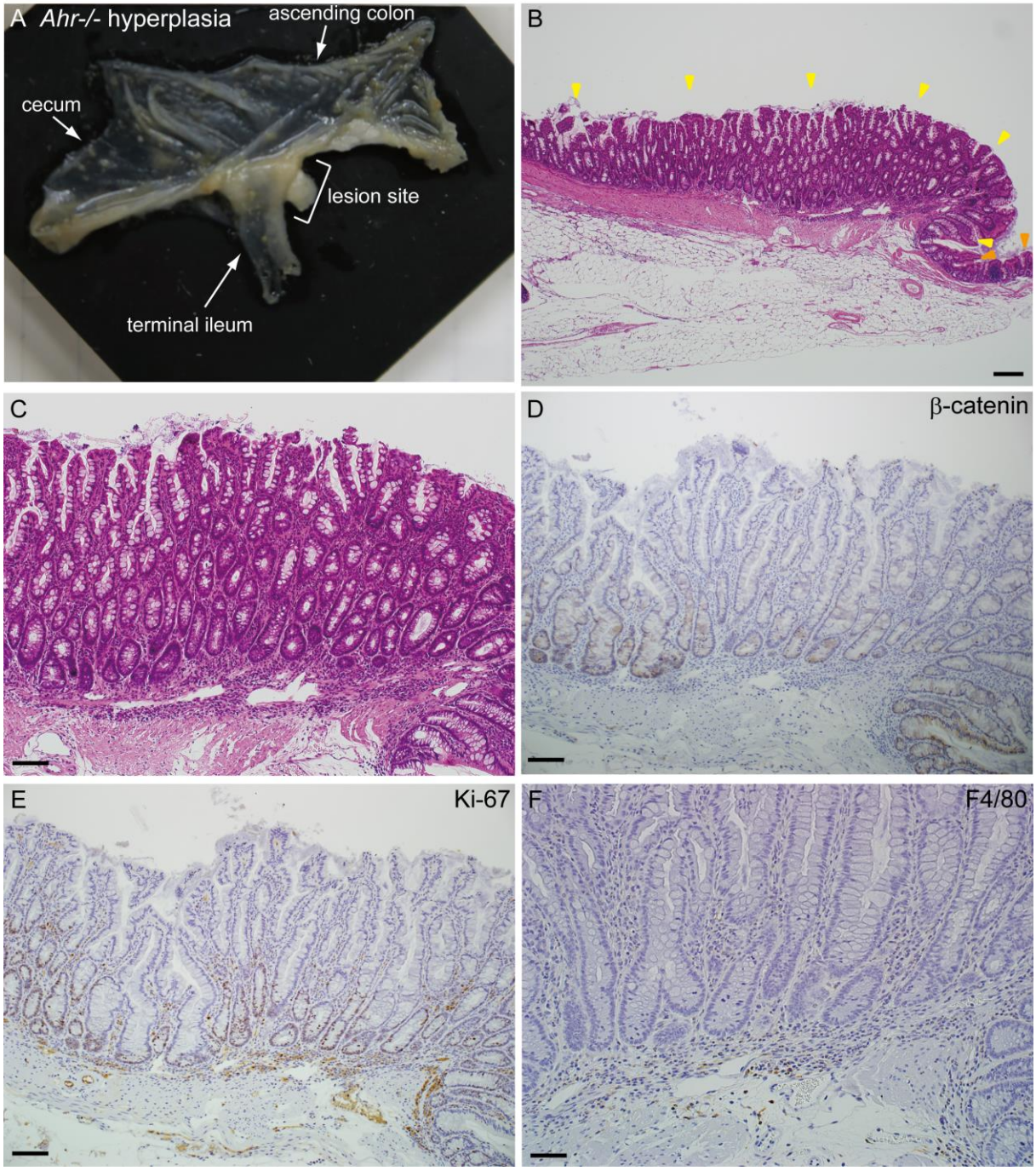

849
850

Figure 3

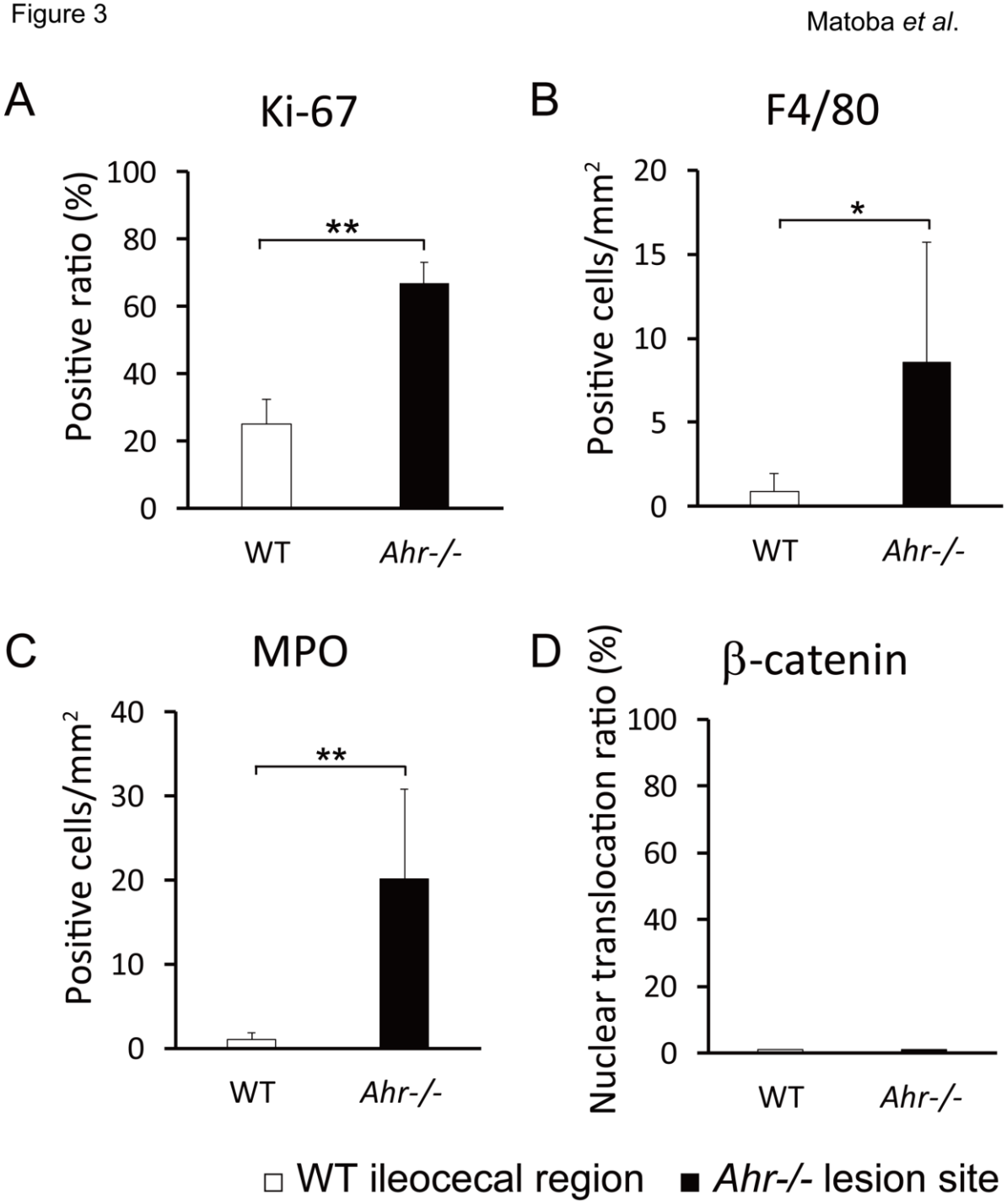

851
852

Figure 4

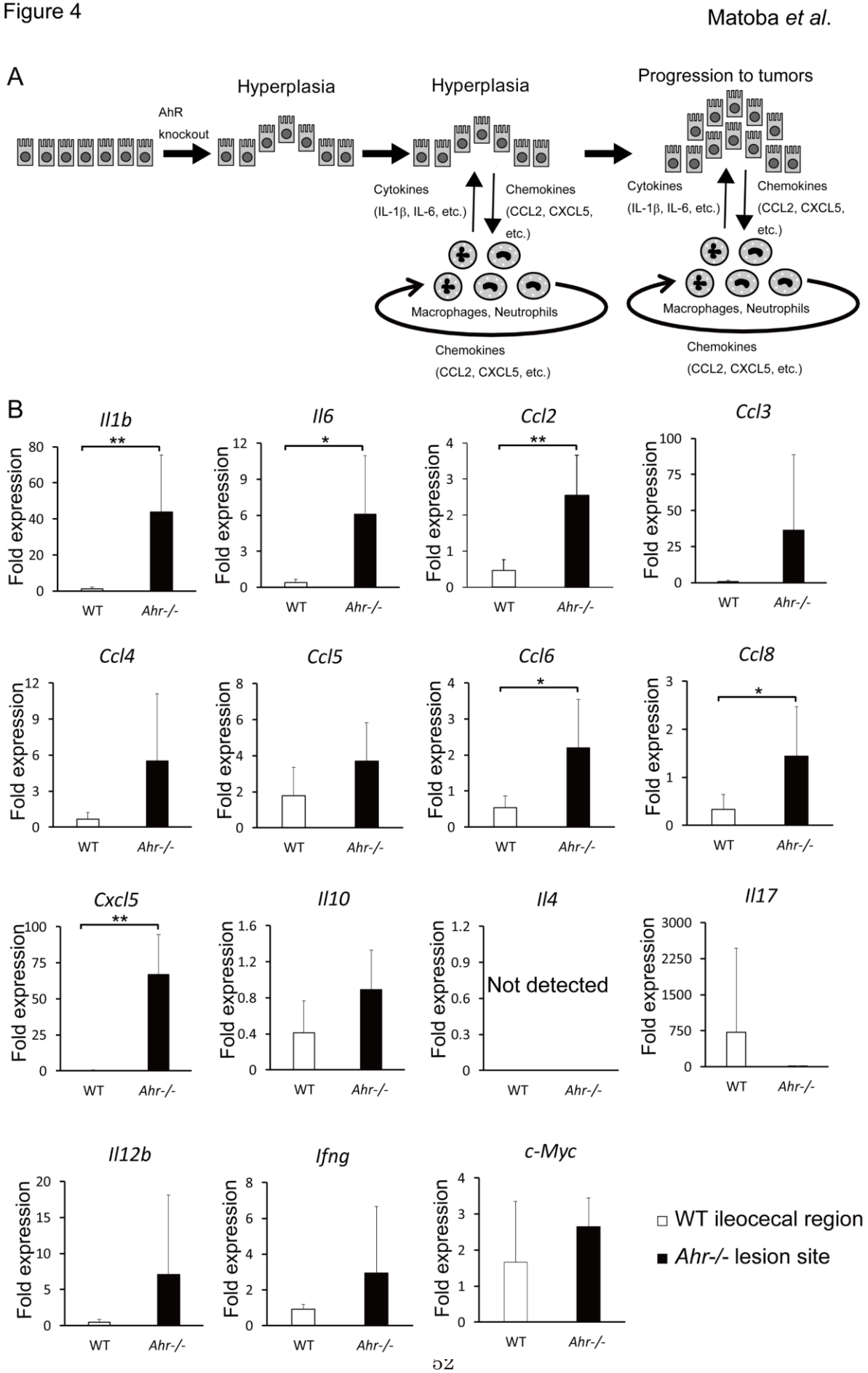
Matoba et al.
A
Hyperplasia
Hyperplasia
Progression to tumors
AhR
knockout
Cytokines
(IL-1β, IL-6, etc.)
Chemokines
(CCL2, CXCL5, etc.)
Macrophages, Neutrophils
Chemokines
(CCL2, CXCL5, etc.)
B
Il1b
Il6
Ccl2
Ccl3
Ccl4
Ccl5
Ccl6
Ccl8
Cxcl5
Il10
Il4
Il17
Il12b
Ifng
c-Myc
Fold expression
WT
Ahr-/-
Not detected
WT ileocecal region
Ahr-/- lesion site

Figure 5

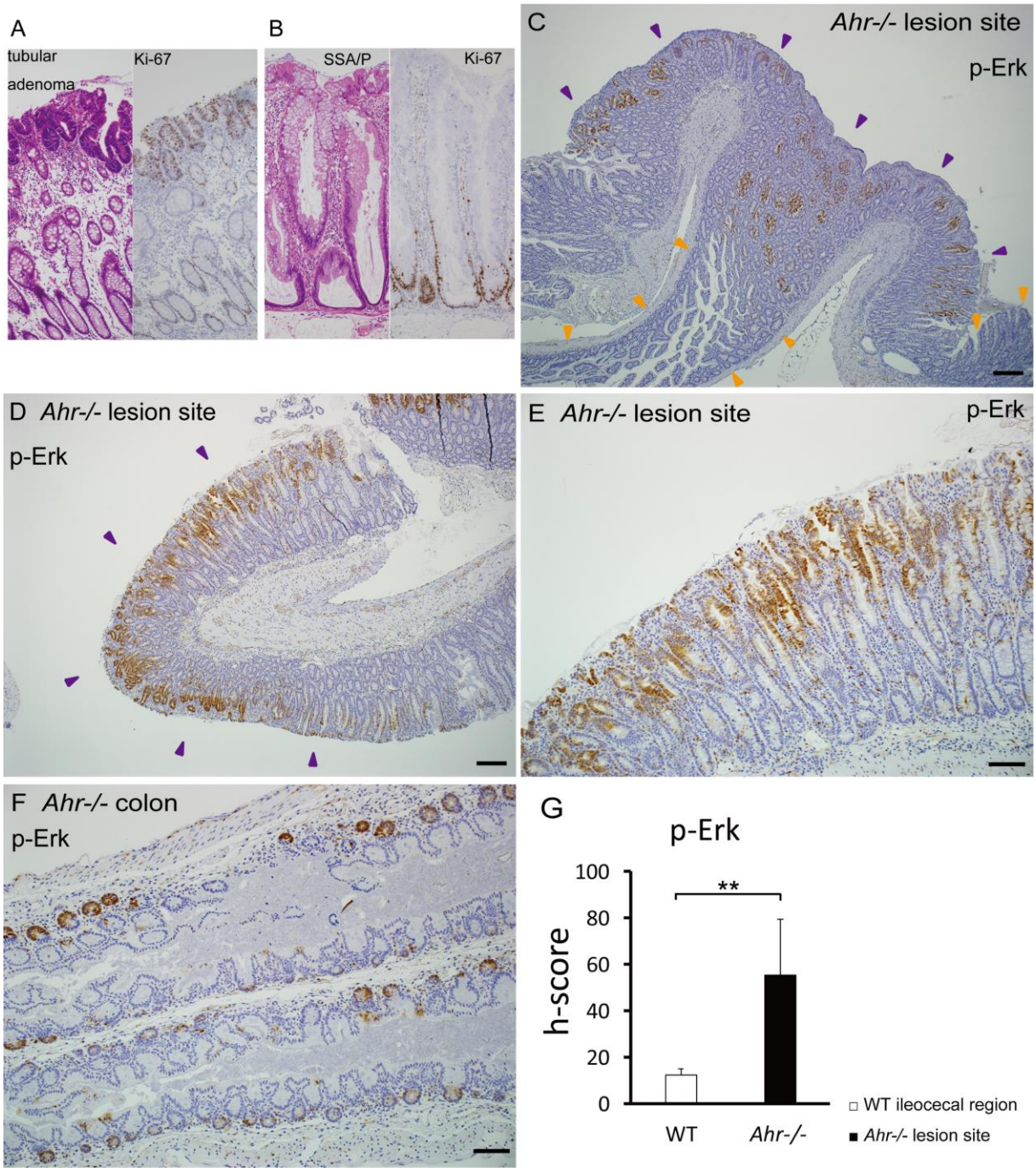

854

855

Figure 6

Matoba *et al.*

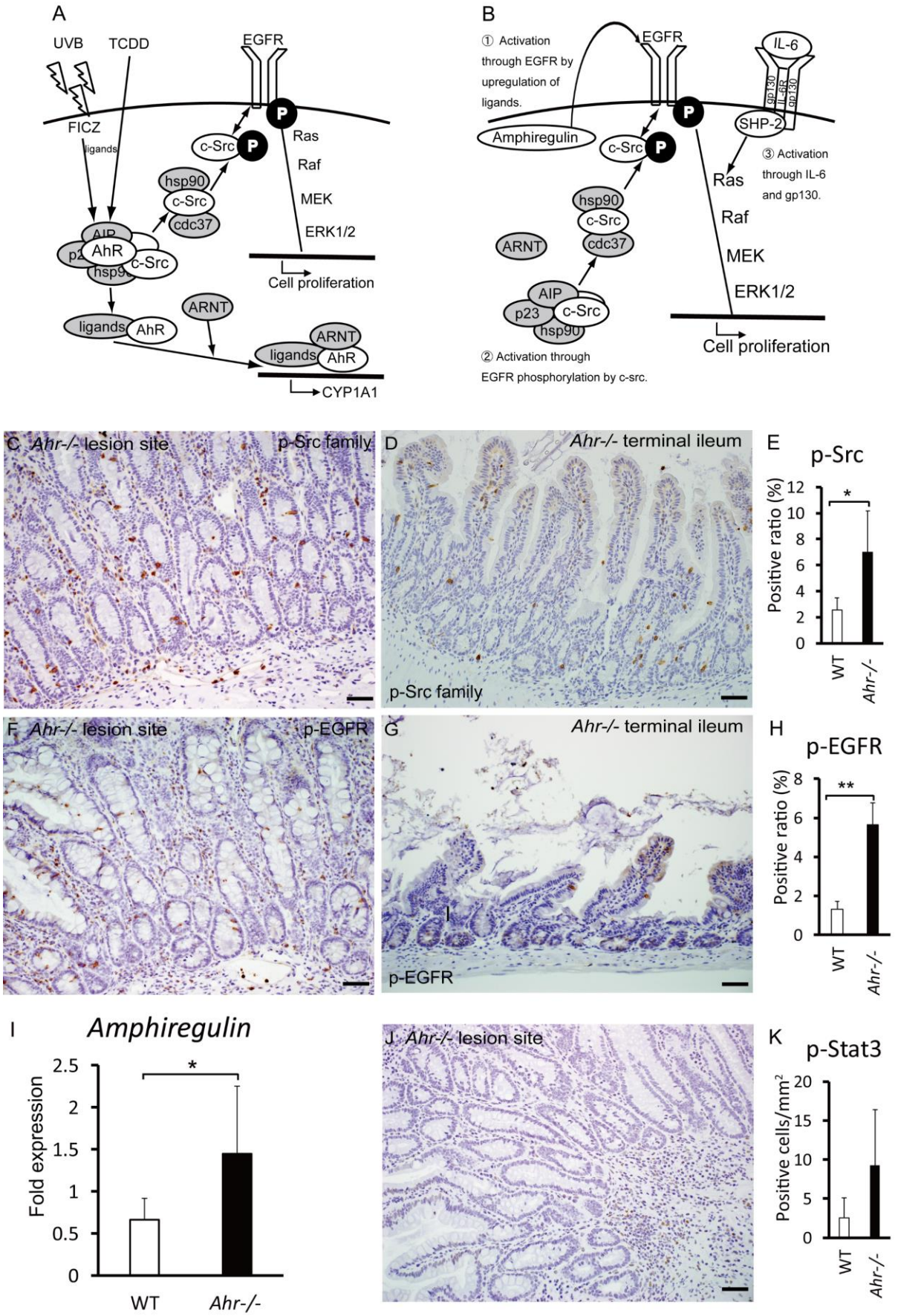

Figure 7

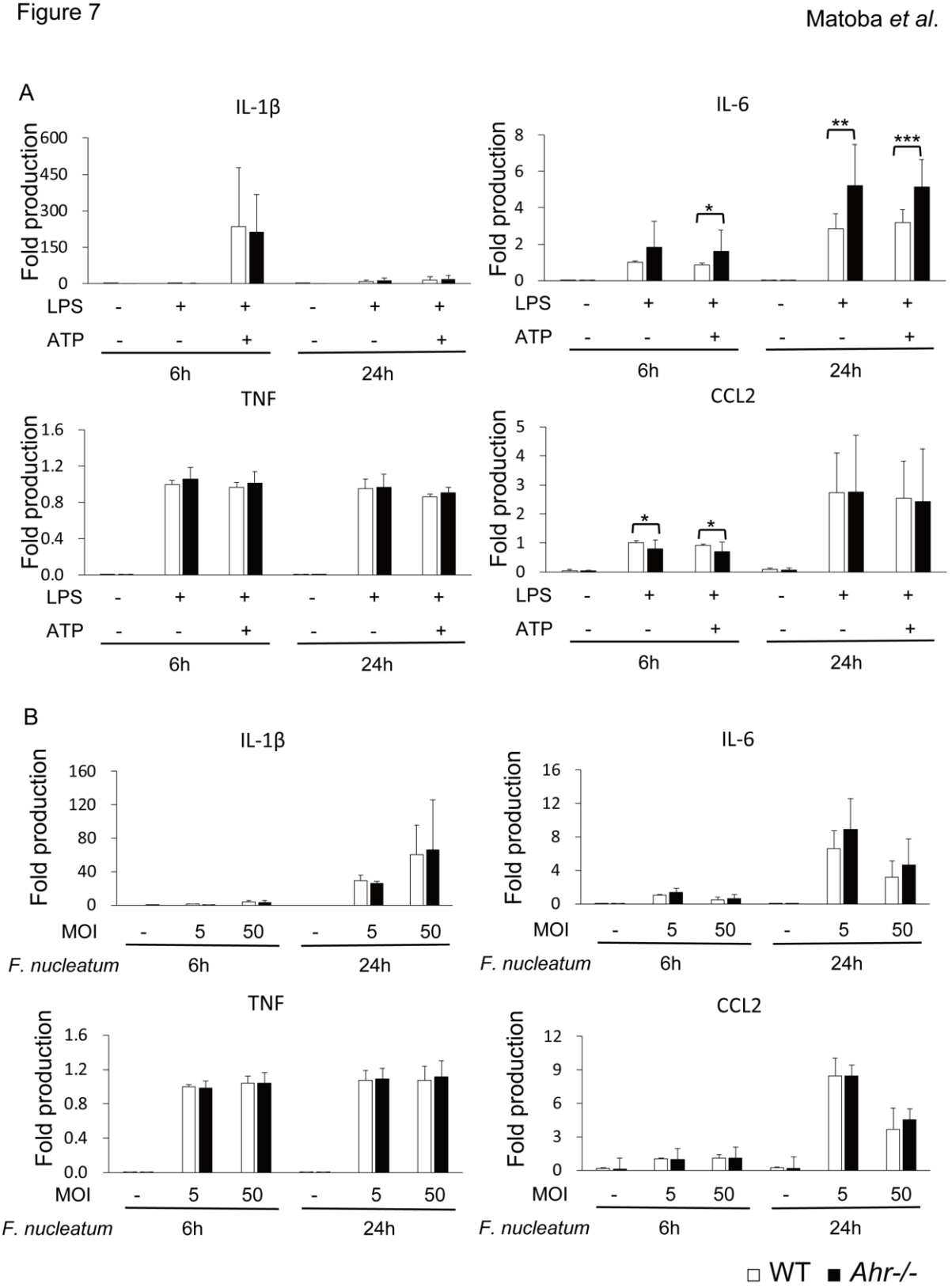
Matoba et al.
A
IL-1β
IL-6
TNF
CCL2
Fold production
LPS
ATP
6h
24h
B
MOI
F. nucleatum
□ WT ■ Ahr-/-

Figure 8

Matoba *et al.*